JOURNAL OF CATALYSIS **170,** 366–376 (1997)
ARTICLE NO. CA971772

Pd/SiO_2-Cogelled Aerogel Catalysts and Impregnated Aerogel and Xerogel Catalysts: Synthesis and Characterization

Benoît Heinrichs,[1] Francis Noville, and Jean-Paul Pirard

Université de Liège, Laboratoire de Génie Chimique, Institut de Chimie au Sart-Tilman-B6a, B-4000 Liège, Belgium

Received December 20, 1996; revised May 27, 1997; accepted June 4, 1997

Pd/SiO_2 aerogel catalysts have been synthesized by cogelation of tetraethoxysilane with complex $Pd^{2+}[NH_2–CH_2–CH_2–NH–(CH_2)_3–Si(OCH_3)_3]_2$ containing a hydrolysable silyl group. Pd catalysts have also been prepared by impregnation of silica aerogels and xerogels with solutions of this complex or $Pd^{2+}(NH_3)_4$ followed by drying under hypercritical conditions or under vacuum. It appears that, in cogelled samples, the Pd^{2+} complex acts as a nucleation agent in the formation of silica particles. The resulting catalysts are then composed of completely accessible palladium crystallites with a diameter of about 2.3 nm located inside silica particles with a monodisperse microporous distribution centered on a hydraulic radius of 0.43 nm. The continuous meso- and macropore distribution is located in voids between particles and between aggregates constituted of those particles. In impregnated samples, it appears that Pd particles are located outside SiO_2 particles. The relation between the texture of cogelled and impregnated catalysts and their behavior toward sintering has been studied in detail. In cogelled samples, it has been shown that Pd crystallites cannot migrate because they are trapped in the pores of SiO_2 particles. These catalysts are sinterproof during hypercritical drying. When Pd crystallites are not trapped inside SiO_2 particles, hypercritical drying leads to an extensive sintering of metal particles. During calcination of impregnated catalysts dried under vacuum, sintering occurs to a various extent depending on the support texture. The Pd crystallites size decreases when the pore size distribution is shifted toward the small sizes.

INTRODUCTION

The synthesis of metallic supported catalysts by the sol–gel route has been examined by numerous authors who showed the ability of this method to highly disperse catalytic metals on gels whose texture is finely controlled. Most of the time, the metal of interest is introduced in the initial solution (whose main components are for example tetraethoxysilane (TEOS) or aluminium tri-sec-butoxide (ATB) and water—with possibly an acid or a base as the gelation catalyst—in alcohol) in the form of a salt (e.g., $PdCl_2$, $Pd(CH_3CO_2)_2$, H_2PtCl_6, $RuCl_3$, etc.) (1–4). In order to homogeneously disperse nanometer-sized metal particles in a silica matrix, Breitscheidel *et al.* (5) prepared modified xerogels by using organically substituted alkoxides of the type $RSi(OR')_3$ where R contains a ligand able to form a chelate with a metal ion such as Pd^{2+}, Pt^{2+}, or Ni^{2+}. This ligand is linked to the hydrolysable silyl group $-Si(OR')_3$ by an inert spacer such as $-(CH_2)_3-$. In this study, $RSi(OR')_3 =$ 3-(2-aminoethyl)aminopropyl-trimethoxysilane, $SiO_3C_8N_2H_{22}$, and the metal is palladium (in the form of palladium acetylacetonate $Pd[CH_3COCH{=}C(O-)CH_3]_2 = Pd(acac)_2$). The introduction of the metal in the silica matrix occurs as shown in Fig. 1. This picture points out the risk of confining the palladium inside the silica matrix and making it inaccessible or difficult to reach for a fluid phase. In impregnated samples, on the contrary, the catalytic metal is spread over the carrier surface only and is completely and easily accessible. If the above complex is used for impregnation, the anchoring of Pd to the silica matrix occurs as shown in Fig. 2. Note that a silica support prepared by the sol–gel process is highly hydroxylated even after thermal treatment (6).

In order to obtain a high porosity (and then perhaps a good accessibility to the active sites), we synthesized gels by the method described in Fig. 1 and dried them under hypercritical conditions to produce aerogel catalysts (7). The main purpose of this study is to examine the dispersion, localization, and accessibility of palladium in cogelled aerogels, the relation between their thermal stability and their texture and the comparison with various catalysts prepared from silica aerogels or xerogels impregnated with solutions containing $Pd^{2+}(SiO_3C_8N_2H_{22})_2$ or $Pd^{2+}(NH_3)_4$.

EXPERIMENTAL

Preparation and Treatment of Samples

Cogelled catalysts. The general method used in this study to produce Pd/SiO_2 cogelled aerogel catalysts has been previously described (5, 8): palladium acetylacetonate powder ($Pd(acac)_2$) and 3-(2-aminoethyl)aminopropyl-trimethoxysilane ($SiO_3C_8N_2H_{22}$) are mixed together in ethanol. The slurry is stirred at room temperature until a

[1] E-mail: bheinric@vml.ulg.ac.be.

0021-9517/97 $25.00

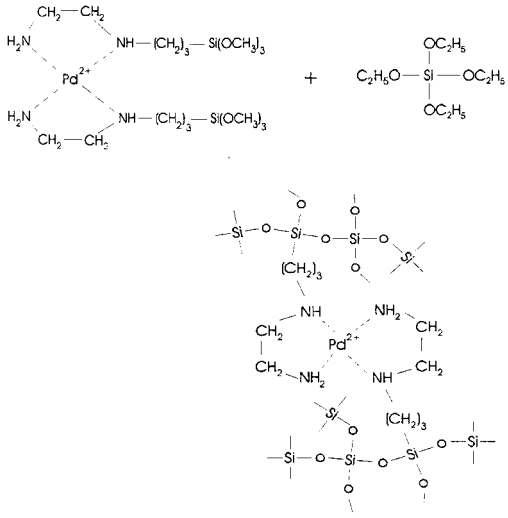

FIG. 1. Introduction of $Pd^{2+}(SiO_3C_8N_2H_{22})_2$ in a silica matrix.

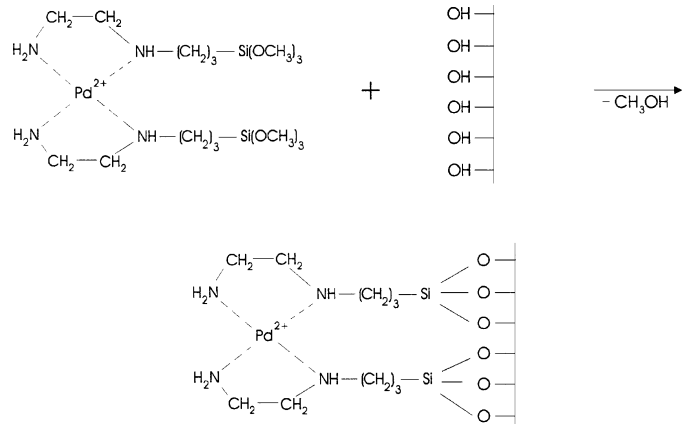

FIG. 2. Impregnation of silica with $Pd^{2+}(SiO_3C_8N_2H_{22})_2$.

clear yellow solution (the color of which is characteristic of palladium complex) is obtained (about half an hour). After addition of tetraethoxysilane (TEOS), a solution of aqueous 0.2*N* NH_3 in ethanol is added to the mixture under vigorous stirring. The vessel is then closed and heated to 70°C for 3 days (gelling and aging (9)). As shown in Table 1, a number of samples with various amounts of reactants have been prepared. In this study, all the cogelled samples were dried in an autoclave under hypercritical conditions for the interstitial liquid in order to avoid interfacial strains which lead to the collapse of the porous texture. In this way, aerogel catalysts with a large pore structure were obtained. Because the interstitial liquid is mainly composed of ethanol, the critical temperature and pressure of the latter ($T_c = 243$°C; $P_c = 6.39$ MPa) have been taken as references. Nevertheless, in order to be sure to exceed the critical point of the interstitial liquid, which can be calculated by a linear combination of the critical parameters of each component (10), we chose a temperature of 327°C and a pressure of 12 MPa.

Impregnated catalysts. Preliminary attempts to synthesize pure silica gels (without $Pd(acac)_2$ and $SiO_3C_8N_2H_{22}$) by the same method as the cogelled samples failed: solutions containing TEOS, H_2O, and NH_3 in ethanol in

TABLE 1

Synthesis Conditions of Cogelled Samples (Aerogels)

Catalyst	$Pd(acac)_2$ (mol/l)	$SiO_3C_8N_2H_{22}$ (mol/l)	TEOS (mol/l)	H_2O (mol/l)	NH_3 (mol/l)	C_2H_5OH (mol/l)	Pd (wt%)	*R*	Gel time (h)
C1	0.000041	0.0005	0.642	3.20	0.012	13.7	0.01	21	—
C2	0.000044	0.1042	0.538	3.20	0.012	13.7	0.01	21	6.5
C3	0.000036	0.6449	0	3.22	0.012	13.8	0.01	21	—
C4	0.000015	0.0174	0.245	1.31	0.005	15.7	0.01	60	7.0
C5	0.000182	0.0004	0.642	3.20	0.012	13.7	0.05	21	—
C6	0.000175	0.1042	0.538	3.20	0.012	13.7	0.05	21	6.5
C7	0.000181	0.6449	0	3.22	0.012	13.8	0.05	21	—
C8	0.000074	0.0174	0.245	1.31	0.005	15.7	0.05	60	7.0
C9	0.000505	0.0010	0.874	4.36	0.016	12.4	0.10	14	10.0
C10	0.000420	0.0008	0.640	3.20	0.012	13.7	0.10	21	48
C11	0.000152	0.0174	0.245	1.31	0.005	15.7	0.10	60	6.0
C12	0.000172	0.0003	0.246	1.23	0.004	15.8	0.10	64	—
C13	0.002490	0.0050	0.873	4.36	0.016	12.4	0.50	14	3.5
C14	0.000758	0.0174	0.245	1.31	0.005	15.7	0.50	60	6.0
C15	0.002131	0.0040	0.640	3.20	0.012	13.7	0.60	21	8.0
C16	0.000807	0.0015	0.246	1.23	0.004	15.8	0.60	64	170
C17	0.003770	0.0074	0.641	3.19	0.011	13.7	1.00	21	8.5
C18	0.007374	0.0147	0.640	3.18	0.011	13.7	2.00	21	2.0
C19	0.008301	0.0153	0.246	1.23	0.004	15.8	5.30	60	2.0

Note. R denotes the dilution parameter $C_2H_5OH/(TEOS + SiO_3C_8N_2H_{22})$, — denotes no gelation after 4 months.

concentrations similar to cogelled samples never gelled. For this reason, pure silica was synthesized by the usual acid–base method (11). The wet silica gel used as the precursor of the support is the same for all impregnated catalysts and is prepared as follows (for 7.5 g of SiO_2): a solution of aqueous 0.1*N* HCl (7.2 ml) in ethanol (40 ml) is added under stirring to a mixture containing TEOS (28 ml) in ethanol (80 ml). The stirring is then stopped and the vessel is closed and maintained at ambient temperature. After 24 h, a solution of aqueous 0.1*N* NH_3 (15.2 ml) in ethanol (40 ml) is added under vigorous stirring. The vessel is then closed and heated to 70°C for 72 h. Wet silica gels have been dried by two different methods: hypercritical drying (as described above for cogelled catalysts) and drying under vacuum at 150°C which leads to xerogels. After drying, all the silica supports were calcined in a flow of dry air at 400°C with an analysis by chromatography of the CO_2 produced to determine the end of calcination. Impregnation solutions are composed of palladium acetylacetonate in ethanol and a ligand which allows the solubilization of palladium. The volume of these solutions corresponds to that of the support. The ligand used is either 3-(2-aminoethyl)aminopropyl-trimethoxysilane or ammonia. Impregnated silica aerogels or xerogels which all contain 2 wt% palladium are dried once again either under hypercritical conditions or under vacuum, after which they are calcined in a flow of dry air at 300°C with an analysis of the CO_2 produced. Synthesis parameters of impregnated samples are shown in Table 2.

Characterization Techniques

Palladium dispersion. Catalysts were examined using a Siemens Elmiskop 102 transmission electron microscope. Suitable transmission samples were prepared by means of an impregnation of gels with an epoxy resin (eurepox 710) to which an amine is added as hardener. Hardening goes on for 48 h after which a 60-nm slice is cut up with a Reichert Supernova ultramicrotome. When the contrast (that is, the gap between gray levels) between palladium particles and silica support was sufficient, photos were examined with image analysis techniques which allow us to obtain a particle size distribution. Palladium dispersion was also determined by carbon monoxide chemisorption. Two methods which differ in the way that they correct for CO physisorption have been applied in two different laboratories. In the first, the calcined sample is reduced at 120°C in hydrogen for 1 h and outgassed at the same temperature for the same length of time. A double CO adsorption is performed at 30°C and at a constant CO pressure of about 57 kPa: the first adsorption includes both physisorption and chemisorption while the second, performed following outgassing, includes physisorption only. The difference between the first and second adsorptions gives the amount of CO chemisorbed (12). In the second, the calcined sample is reduced in flowing hydrogen at 120°C for 1.5 h and at 110°C for 16 h, and a CO adsorption isotherm is measured at 30°C on a Fisons Sorptomatic 1990 device. The amount of CO chemisorbed is obtained by extrapolating the isotherm to zero pressure to correct for physisorption (13–15).

Catalyst textures. Nitrogen adsorption isotherms at 77 K were obtained using a Carlo Erba Sorptomatic 1990 (after outgassing at 100°C for 4 h). Specific surface areas and pore size distributions were then calculated following the methodology proposed by Lecloux (16). Mercury porosimetry was performed with a Carlo Erba Porosimeter 2000 on samples outgassed at ambient temperature for 4 h to determine their porous volumes.

RESULTS

Synthesis

Synthesis parameters of cogelled samples (denoted by the letter C) are shown in Table 1. Gel time is the time elapsed between the introduction of the liquid solution in the oven at 70°C and gel formation, determined at the time when the liquid does not flow when tilted. Hydrolysis molar ratio $h = H_2O/(TEOS + \frac{3}{4}SiO_3C_8N_2H_{22})$ (the factor $\frac{3}{4}$ is due to the fact that $SiO_3C_8N_2H_{22}$ contains only three hydrolysable groups in relation to TEOS which contains four hydrolysable groups) is kept constant at a value of 5 for all cogelled catalysts. The comparison between samples C1 and C2; C5 and C6; C12 and C11; and C16 and C14 which are characterized, in each pair, approximately by the same

TABLE 2

Synthesis Conditions of Impregnated Samples

Catalyst	Support	$Pd(acac)_2$ (mol/l)	Ligand Nature	Ligand (mol/l)	H_2O (mol/l)	C_2H_5OH (mol/l)	Pd (wt%)	Drying
I1	Aerogel	0.0072	$SiO_3C_8N_2H_{22}$	0.014	0	17.1	2	Hypercritical
I2	Aerogel	0.0065	$SiO_3C_8N_2H_{22}$	0.013	0	17.1	2	Vacuum
I3	Aerogel	0.0059	NH_3	0.047	1.4	16.7	2	Vacuum
I4	Xerogel	0.0741	$SiO_3C_8N_2H_{22}$	0.148	0	16.6	2	Vacuum
I5	Xerogel	0.0726	NH_3	0.582	17.8	11.0	2	Vacuum

TABLE 3

Pd Average Particle Size and Dispersion

Catalyst	Metal loading (wt%)	TEM d (nm)	TEM σ (nm)	CO chemisorption d (nm)	CO chemisorption D (%)
C10	0.1	2.4[a]	0.4	—	—
C13	0.5	2.3[a]	0.4	—	—
C18	2	2.0[a]	0.3	2.4	47[c]
				2.2	51[d]
C19	5.3	80.9[b]	24.0	—	—
I1	2	24.6[b]	1.5	16.8	7[d]
I2	2	7.5[b]	1.5	—	—
I3	2	7.3[b]	1.9	—	—
I4	2	4.4[b]	1.2	—	—
I5	2	5.0[b]	1.9	—	—

Note. d denotes the mean diameter of Pd particles measured by TEM or chemisorption; σ the standard deviation; D, the metal dispersion measured by chemisorption; —, not measured.

[a] Visual evaluation was used.

[b] Image analysis was used.

[c] Double adsorption.

[d] Adsorption isotherm.

parameters, except the concentration of $SiO_3C_8N_2H_{22}$ indicates that an increase in the ligand concentration makes gelation possible (three first pairs) or decreases the gelling time (fourth pair). Concerning the influence of the dilution parameter R which is defined as the molar ratio $C_2H_5OH/(TEOS + SiO_3C_8N_2H_{22})$, the gel time increases with R (comparison between samples C9, C10, and C12; C13, C15, and C16).

The synthesis conditions of the impregnated samples (denoted with the letter I) are shown in Table 2. In catalysts I1, I2, and I4, the molar ratio $SiO_3C_8N_2H_{22}/Pd(acac)_2$ is 2 (this corresponds to the palladium coordination number which is 4), whereas in samples I3 and I5, the molar ratio $NH_3/Pd(acac)_2$ is 8. The two ligands have been used so as to check the interest of anchoring groups in $SiO_3C_8N_2H_{22}$ for palladium dispersion in impregnated catalysts. Drying of impregnated gels has been performed either by hypercritical extraction or under vacuum in order to study the influence of drying conditions on final support texture and palladium particle-size distribution.

Dispersion and Localization of Palladium

Table 3 shows the palladium particle size as measured by TEM and CO chemisorption. Because of a weak contrast in the TEM pictures between Pd particles and the SiO_2 support in samples C10, C13, and C18, binarization of photos was impossible and sizes have been evaluated by a visual appreciation on 50 particles. The sizes obtained for samples C19 and I1 are mean values (obtained by image analysis) on only 13 and 6 particles respectively because of their large sizes and consequently their small number. For samples I2 to I5, mean values are obtained from distributions on 70 to 200 particles determined with image analysis techniques on TEM pictures. In order to calculate the dispersion D (that is, the atomic ratio between the number of surface Pd atoms (Pd_s) and the number of total Pd atoms) from CO chemisorption measurements, the stoichiometric ratio CO/Pd_s has to be known. It has been shown that CO chemisorption on Pd can occur in two ways (17, 18): a carbon monoxide molecule can be bonded through the carbon to one Pd atom (linear CO) or to two Pd atoms (bridged CO). The ratio of linearly held CO to bridged-bonded CO decreases as the dispersion decreases (19, 20) and the result of this is an increase in the global ratio CO/Pd_s with dispersion. Joyal and Butt (21) have determined CO/Pd_s ratios as a function of dispersion on Pd/SiO_2 catalysts. Assuming Pd particles to be roughly spherical in shape, metal dispersion was calculated from TEM measurements for samples subjected to chemisorption. Those values have then been used to choose the right CO/Pd_s ratios determined by Joyal and Butt. The following ratios were selected: sample C18, $CO/Pd_s = 0.74$; sample I1, $CO/Pd_s = 0.5$. These values were used to estimate dispersion and particle diameters from the CO chemisorption measurements given in Table 3.

The results clearly show that the smallest Pd particles are obtained for cogelled catalysts (around 2.2 nm in samples C10, C13, and C18). Nevertheless, under some conditions, very low dispersions are obtained (80.9 nm in sample C19). Impregnated catalysts exhibit Pd particles at least twice the size of the cogelled catalysts. Hypercritical drying following impregnation leads to a low dispersion as shown in sample I1. A comparison between samples I2, I3 (aerogel support) and I4, I5 (xerogel support) shows a higher dispersion for catalysts prepared from xerogels. The nature of the ligand (which changes from I2 to I3 and from I4 to I5) does not strongly influence the mean Pd particle size but influences the broadening of the size distribution (quantified by standard deviation σ in Table 3) as shown in Fig. 3 (which show distributions for samples I4 and I5; note that similar effects

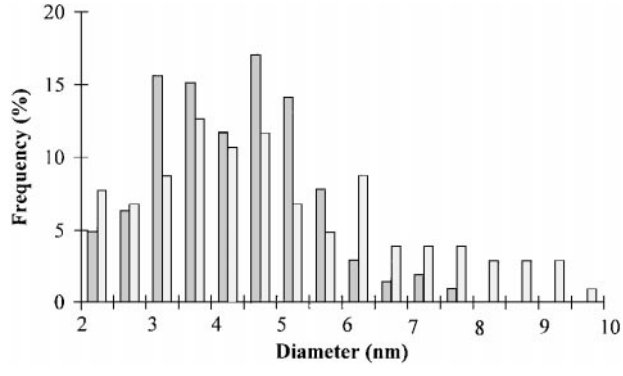

FIG. 3. Paladium particle size distribution in samples I4 and I5 determined by TEM and image analysis (, I4; , I5).

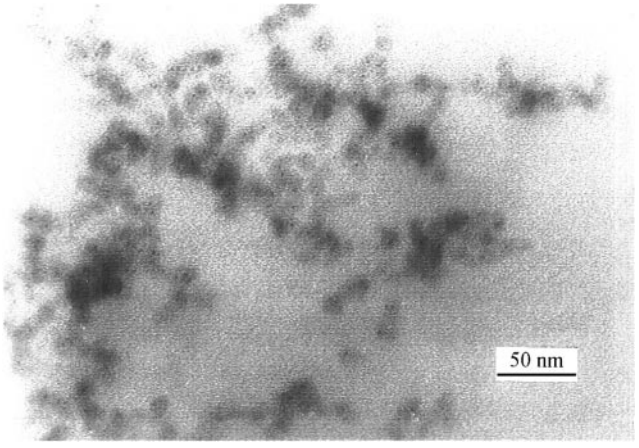

FIG. 4. TEM micrograph of sample C18 (200,000×).

are observed for samples I2 and I3): the use of $SiO_3C_8N_2H_{22}$ instead of NH_3 leads to a higher monodispersity of the Pd particle size distribution. One has to note the good agreement between TEM and chemisorption for samples C18 and I1 knowing that, in the latter, the mean diameter obtained by TEM is not precise because of the crystallites' small number. It should also be noted that the double adsorption technique gives nearly the same results for sample C18 as the extrapolation to zero pressure method.

Although TEM gives only a 2D view, a careful examination of cogelled-catalyst TEM pictures, an example of which is given in Fig. 4 with catalyst C18, shows that, except for sample C19 which is characterized by the greatest metal loading, Pd particles appear to be located inside the silica particles. In contrast, in C19 and impregnated samples, an example of which is given in Fig. 5 with catalyst I1, Pd is located on the surface of silica network. This palladium localization is of importance to the behavior of samples examined here in relation to sintering and will be discussed in detail below.

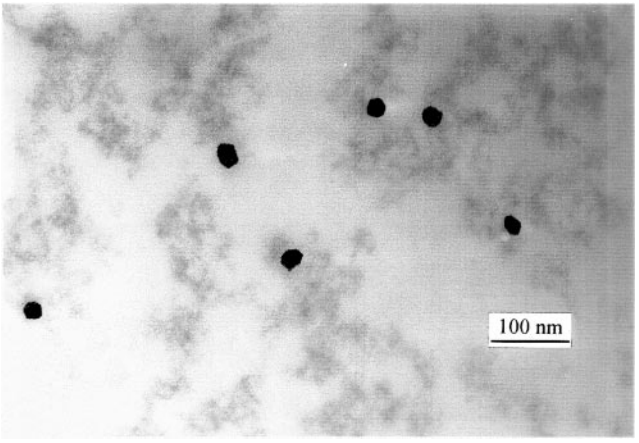

FIG. 5. TEM micrograph of sample I1 (100,000×).

TABLE 4

Texture of Cogelled Catalysts (Not Calcined)

Catalyst	S_{BET} (m^2/g)	S_t (m^2/g)	$r_{h\ micro}$ (nm)	V_0 (cm^3/g)	V_{Hg} (cm^3/g)
C10	297	301	0.44	0.13	9.5
C13	196	196	0.42	0.09	—
C18	255	256	0.44	0.12	25.0
C19	431	432	0.45	0.19	20.2

Note. S_{BET} denotes the specific surface area obtained by N_2 adsorption and BET method; S_t the specific surface area obtained by N_2 adsorption and *t*-plot method; $r_{h\ micro}$ the micropore hydraulic radius; V_0 the specific micropore volume calculated by the Dubinin–Raduskevitch method; V_{Hg} the specific pore volume measured by Hg porosimetry. — denotes no measure.

Texture of Catalysts

Cogelled catalysts. The texture of samples C10, C13, C18, and C19 has been examined in detail and the results are shown in Table 4 and Figs. 6–7. The nitrogen adsorption isotherms of the cogelled catalysts belong to type II in the classification proposed by Brunauer *et al.* (22) which is observed for adsorbents containing macropores (width >50 nm (23)) (Fig. 6). The *t*-plots (24, 25) are also similar for all cogelled samples. They always show a downward deviation which is characteristic of micropores (width <2 nm (23)) followed by an upward deviation which is characteristic of mesopores (2 nm < width < 50 nm (23)) (Fig. 7). The presence of mesopores is evidenced by the calculation of the pore size distributions in the mesopore range by the Broekhoff–de Boer method (26–28) which shows a continuous distribution for diameters between 2 and 50 nm. The cogelled samples then contain micro-, meso-, and macropores, which is a characteristic of aerogels (29). The domain in the *t*-plots before the upward deviation deserves careful examination. It appears indeed that this part of the plot can be represented by two straight lines whose intersection corresponds, for the four samples examined, to almost the same value of the thickness *t* of the adsorbed nitrogen

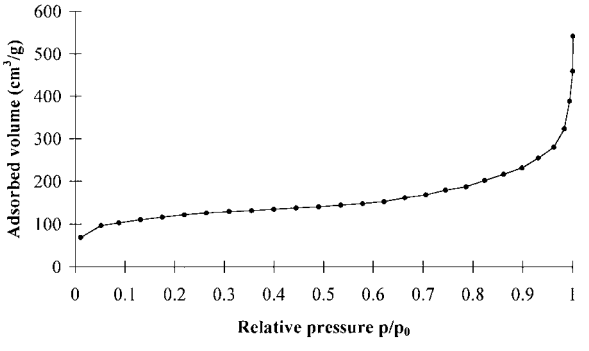

FIG. 6. N_2 adsorption isotherm on sample C19.

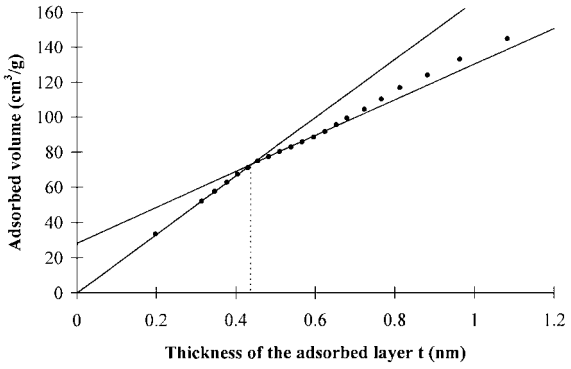

FIG. 7. *t*-plot of sample C18.

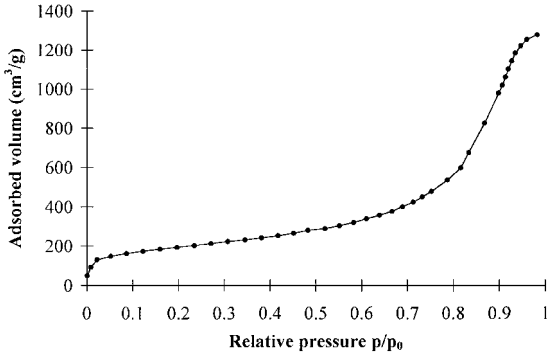

FIG. 8. N_2 adsorption isotherm on sample I3.

layer, which is about 0.43 nm. The use of Brunauer's method to calculate the micropore size distribution (30, 31) by the downward deviation in the *t*-plot leads then to a monodisperse distribution. The hydraulic radius of the micropores (that is, the ratio between the pore volume and its surface), $r_{h\,micro}$, is about 0.43 nm.

Mercury porosimetry applied to cogelled samples (32–34) shows a continuous pore size distribution between the largest macropores and the mesopores with a diameter greater than about 7.5 nm, which is the lower limit of the method.

As previously observed (5), a comparison between S_{BET} before and after calcination of the cogelled sample C18 indicates that burning of the organic residues frees the pores and leads to a significant increase of the specific surface area from 255 to 392 m^2/g.

Impregnated catalysts. Textural properties of impregnated samples are shown in Table 5 and Figs. 8 and 9. Catalyst I1 exhibits a type-II isotherm observed for adsorbents containing macropores whereas catalysts I2 to I5 exhibit type-IV isotherms characteristic of adsorbents which contain mesopores (Fig. 8). The *t*-plots always present an upward deviation showing the presence of mesopores. This mesoporosity also appears in pore size distributions calculated by means of the Broekhoff–de Boer method which shows an important difference between samples I1, I2, and I3 on the one hand and samples I4 and I5 on the other. While the former exhibit a continuous distribution in the mesoporous range, the latter do not have any mesopores with diameter larger than approximately 15 nm (Fig. 9).

The porous volumes V_{Hg} (Table 5) determined by mercury porosimetry confirm the results obtained by nitrogen adsorption. A comparison of the porous volumes of catalysts I1, I2, and I4 clearly shows that hypercritical drying is a way to retain high porosity even in sample I2 dried under vacuum after impregnation of the aerogel support and which has a porous volume six times greater than that of I4 dried twice under vacuum.

A comparison between cogelled and impregnated catalysts and between impregnated catalysts dried twice under hypercritical conditions (I1), once under hypercritical conditions and once under vacuum (I2 and I3), or twice under vacuum (I4 and I5) indicates that drying under vacuum leads to samples characterized by higher micropore volumes V_0 calculated by the Dubinin–Raduskevitch method (16) and then by higher specific surface areas S_{BET}.

To summarize, drying under vacuum, in relation to hypercritical drying, leads to the decrease or the disappearance of macropores and large mesopores and favors the

TABLE 5

Texture of Impregnated Catalysts (Calcined)

Catalyst	S_{BET} (m^2/g)	S_t (m^2/g)	V_0 (cm^3/g)	V_{Hg} (cm^3/g)
I1	763	789	0.28	17.6
I2	750	767	0.31	4.1
I3	703	712	0.29	—
I4	909	927	0.39	0.7
I5	879	893	0.32	—

Note. S_{BET} denotes the specific surface area obtained by N_2 adsorption and BET method; S_t the specific surface area obtained by N_2 adsorption and *t*-plot method; V_0 the specific micropore volume calculated by the Dubinin–Raduskevitch method; V_{Hg} the specific pore volume measured by Hg porosimetry. — denotes no measure.

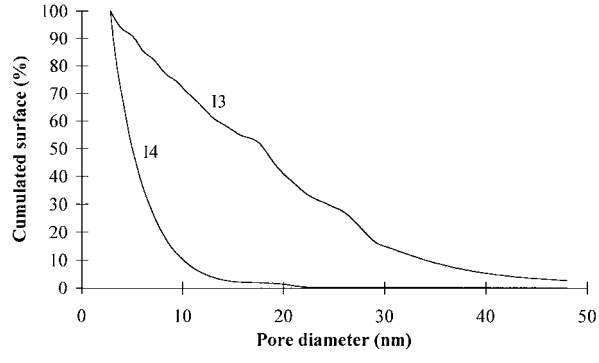

FIG. 9. Mesopore size distribution in samples I3 and I4.

micropores' appearance. These observations are in agreement with the conclusions of Brinker and Scherer (9) who noted that the large scale structure of gels is weak and easily collapses by capillary pressure during drying under vacuum, whereas the micropores and mesopores that produce the high surface area are present in a more rigid network.

As for cogelled catalysts, it has been shown in the case of sample I1 that calcination leads to an increase of S_{BET} from 656 to 763 m^2/g.

DISCUSSION

In cogelled samples, 3-(2-aminoethyl)aminopropyl-trimethoxysilane ($SiO_3C_8N_2H_{22}$) appears not only as a ligand for palladium but also as a catalyst which has a marked influence on the kinetics of sol–gel reactions. Results in Table 1 show that $SiO_3C_8N_2H_{22}$ increases the reaction rates. Containing two amines, this compound can be assumed to act as a base catalyst like NH_3 and thus increases the hydrolysis and condensation rates (35). An attempt to synthesize a catalyst by replacing all TEOS with $SiO_3C_8N_2H_{22}$ has been performed. While a heat emission indicating that hydrolysis of $SiO_3C_8N_2H_{22}$ occurs is clearly observed, no gelation was observed after 4 months. This result shows that there is probably an optimal concentration of $SiO_3C_8N_2H_{22}$ where gelation is the fastest. One can explain this optimum by assuming the existence of two antagonistic effects: on the one hand, the ligand increases the reaction rates thanks to its catalytic power; and on the other hand, because of its steric cluttering, it slows down the condensation reaction.

After drying, sol–gel catalysts still contain many organic compounds which can be burned by oxidation at high temperature. It is interesting to point out that an analysis of carbon dioxide produced during calcination indicates that the emission of CO_2 starts at about 200°C for Pd catalysts, whereas it usually starts at about 300°C for similar samples without Pd. This gap can be explained by the oxidation power of Pd which activates calcination. In the case of the cogelled sample C18 (which is the only cogelled catalyst a fraction of which has been calcined for CO chemisorption), this effect is a first indication of the accessibility, or at least partial accessibility, of the active centers.

An important advantage of the cogelation method is the possibility of homogeneously distributing the catalytic metal through the whole material, that is, inside the silica particles, contrary to the impregnation method which leads to a metal distribution on the particle surface only (36). This is evidenced by TEM micrographs. Cogelled samples (except C19) seem indeed to exhibit palladium particles located inside the silica matrix, whereas impregnated samples show metal particles located outside the silica matrix (Figs. 4 and 5). The palladium localization inside silica particles in cogelled samples is probably a consequence of the ligand used: the hydrolyzable functions in $SiO_3C_8N_2H_{22}$ allow the formation of Si–O–Si bonds all around the complex (Fig. 1) and the observation of Fig. 4 suggests that this complex or a group of such molecules can act as a nucleation agent which leads after all to silica particles with a palladium heart. In order to assess the validity of this nucleation by palladium complex hypothesis, the relation between SiO_2 particle volume and TEOS and $SiO_3C_8N_2H_{22}$ and Pd concentrations has been examined. Expressing that the volume occupied by the silica skeleton is proportional to the sum of TEOS and $SiO_3C_8N_2H_{22}$ concentrations, one obtains:

$$N_p V_p (1-\varepsilon) = C_1\big([\mathrm{TEOS}] + [\mathrm{SiO_3C_8N_2H_{22}}]\big) \qquad [1]$$

where N_p is the number of SiO_2 particles in the gel, V_p is the volume of one SiO_2 particle (nm^3), and ε is its void fraction. C_1 is a constant. [TEOS] and [$SiO_3C_8N_2H_{22}$] are the concentrations of TEOS and $SiO_3C_8N_2H_{22}$ (mol/l). The nucleation by palladium complex hypothesis leads to:

$$N_p = C_2[\mathrm{Pd^{2+}}], \qquad [2]$$

where C_2 is a constant ($1/C_2$ is proportional to the Pd atomic number in one nucleus). [Pd^{2+}] is the concentration of the Pd complex (mol/l). Combining [1] and [2] and assuming that ε has the same value in all SiO_2 particles, one obtains:

$$V_p = C_3\big([\mathrm{TEOS}] + [\mathrm{SiO_3C_8N_2H_{22}}]\big)/[\mathrm{Pd^{2+}}] \qquad [3]$$

where $C_3 = C_1/(C_2(1-\varepsilon))$. Finally,

$$d_p^3 = C_4\big([\mathrm{TEOS}] + [\mathrm{SiO_3C_8N_2H_{22}}]\big)/[\mathrm{Pd^{2+}}], \qquad [4]$$

where d_p is the diameter of SiO_2 particles (nm) and $C_4 = 6C_1/(\pi C_2(1-\varepsilon))$.

d_p has been measured by TEM for samples C10, C13, C18, and C19 and the ratio $([\mathrm{TEOS}] + [\mathrm{SiO_3C_8N_2H_{22}}])/[\mathrm{Pd^{2+}}]$ has been calculated with values given in Table 1. Results are shown in Table 6 and Fig. 10. One observes that relation (4) adequately represents experimental data with $C_4 = 7.2$. That result combined with TEM observations reinforces the nucleation by Pd^{2+} hypothesis.

It can then be reasonably assumed that gel formation occurs via SiO_2 particle nucleation by a set of Pd^{2+} complexes,

TABLE 6

SiO_2 Particle Volume versus ([TEOS] + [$SiO_3C_8N_2H_{22}$])/[Pd^{2+}] Ratio

Catalyst	$\frac{([\mathrm{TEOS}] + [\mathrm{SiO_3C_8N_2H_{22}}])}{[\mathrm{Pd^{2+}}]}$	d_p (nm)	d_p^3 (nm^3)
C10	1526	22.2	10941
C13	353	14	2744
C18	89	9.7	913
C19	31	7	343

Note. d_p denotes the SiO_2 particle diameter measured by TEM.

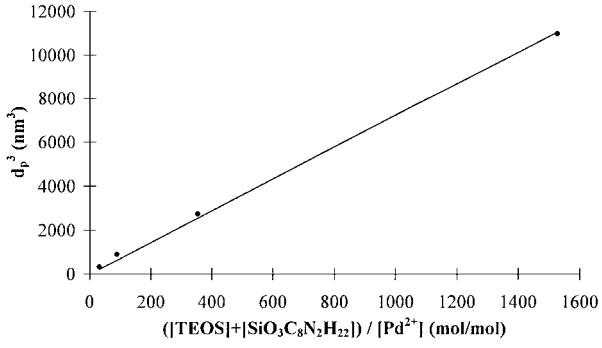

FIG. 10. Silica particle nucleation by Pd^{2+} complex.

particles growing thanks to hydrolysis and condensation of methoxy groups of $SiO_3C_8N_2H_{22}$ and TEOS, and finally particle aggregation.

A very important concern about cogelled catalysts is the accessibility of the active centers. Because palladium is located inside silica particles, there is a risk that it may not be accessible. By performing drying under hypercritical conditions, the goal is to maintain the macro- and mesoporosity, and thus the accessibility, as high as possible. The values of V_{Hg} in Table 4 show that the ability of this drying to retain porosity is high, but do not prove the accessibility of palladium. The activity of the cogelled catalyst C10 for hydrogen combustion has been measured at 20°C and 1 atm with a mixture containing 3% hydrogen in air. The turnover frequency of 102 s^{-1} obtained (number of molecules of water produced per surface Pd atom per second) indicates that small molecules such as H_2 and O_2 can reach the metal. Provided that the ratio $CO/Pd_s = 0.74$ chosen for catalyst C18 is sufficiently close to the real mean stoichiometry and Pd particles are more or less spherical, the agreement between TEM and chemisorption results in Table 3 is, for this cogelled sample, the proof that all Pd particles are accessible for CO and then for any reactants (provided that the molecules are not too large) in a catalytic system.

The fact that, in catalysts C10, C13, and C18, palladium is accessible and located inside silica particles leads to the obvious conclusion that these particles are porous. Knowing, moreover, as demonstrated by the textural analysis, that those samples exhibit a monodisperse pore size distribution in the microporous domain and a continuous distribution in the mesoporous and macroporous domains, it is reasonable to assume the following structure for cogelled catalysts: palladium particles with a diameter of about 2.2 nm would be located inside quasi-monodisperse porous silica particles whose diameter is between 9.7 and 22.2 nm, depending on the sample. Those SiO_2 particles show a monodisperse microporous distribution centered on a hydraulic radius $r_{h\ micro}$ equal to 0.43 nm. The continuous meso- and macroporous distribution would be located in voids between these particles and between aggregates constituted of these particles. Due to their huge size (∼80 nm), palladium particles in sample C19 are of course located outside silica particles the size of which is 7 nm.

The difference between Pd particle sizes in catalysts I1, and I2, which are impregnated aerogels dried under hypercritical conditions and under vacuum, respectively, suggests that hypercritical drying can lead to an important sintering of palladium. This phenomenon seems not to occur (except in sample C19) in cogelled catalysts.

Sintering of supported metal catalysts has been studied in detail by Ruckenstein and co-workers (37). These authors suggested three mechanisms for sintering: (a) migration of crystallites on the support and their coalescence (38–40; (b) Ostwald ripening that is the emission of single metal atoms and multiatom particles from larger particles, their diffusion along the substrate, and the coalescence of particles (or of a particle and an atom) that collide (41); (c) direct ripening where single atoms are transferred directly from a smaller to a larger particle if they are sufficiently near to each other (42). Experimental studies showed that migration and coalescence and ripening mechanisms can occur and that one of them can be dominant depending on the conditions (43, 44). Migration and coalescence is more likely to occur in metal catalysts on an oxide support since, in this case, the bonding energies of metal atoms to metal crystallites are much larger than the bonding energies of metal atoms to the support which makes the dissociation between metal atoms and metal crystallites unlikely (38). On the contrary, Ostwald ripening is more likely to occur in metal oxide catalysts on an oxide support due to the greater emission capability of the oxides in relation to the metals on oxide substrates (37). In conclusion, a reducing atmosphere favors migration and coalescence whereas an oxidizing atmosphere favors Ostwald ripening.

When the sintering of supported metal catalysts is caused by migration and coalescence, the crystallite diffusion on the surface of the substrate can be impeded by the porous texture if the crystallites sizes are of the order of magnitude of the pore diameters (45). Zou and Gonzalez have recently examined the thermal stability of Pd/SiO_2 sol–gel catalysts (46). One of their observations is the following: when the average particle size coincides with the average pore diameter, the Pd particles are found to be stable at temperatures of up to 650°C for 22 h in an oxygen atmosphere. According to these authors, at this temperature, the primary mechanism for particle growth is the surface migration of PdO in an oxidizing atmosphere which is inhibited when the size of crystallites reaches the size of pores. For an unknown reason, treatment in hydrogen at the same temperature resulted in considerable Pd sintering. Although the influence of the atmosphere is not well understood, those results clearly confirm that the final crystallite size distribution can be strongly affected by the porous texture.

During drying in an autoclave, gels are placed in a hypercritical fluid composed mainly of ethanol. Under this reducing atmosphere at 327°C, it can be reasonably assumed that Pd^{2+} cations trapped in complexes are transformed in Pd^0. This results in the formation of metal crystallites which are observed by TEM in noncalcined samples (Fig. 4). This drying then combines the conditions which favor the migration and coalescence mechanism: a metal catalyst on an oxide support under reducing atmosphere and high temperature which enhances the crystallite mobility. In the case of cogelled samples C10, C13, and C18, it has been shown that Pd crystallites have a diameter of about 2.2 nm and are located inside SiO_2 particles. The latter exhibit a monodisperse micropore distribution centered on a hydraulic radius $r_{\text{h micro}}$ equal to 0.43 nm. It can be assumed that the value of 2.2 nm for the Pd particle diameter obtained with dried samples corresponds to the diameter of particles just formed after Pd^{2+} reduction in the autoclave. Pd crystallites would also be observed on the surface of SiO_2 particles if there were migration and coalescence of smaller metal particles. The hydraulic radius being equal to 0.43 nm, the characteristic width of the micropores is smaller than that of the Pd particles. It appears then that in samples C10, C13, and C18, it is impossible for Pd crystallite to migrate outside the silica particle and it can be concluded that those cogelled samples are sinter-proof during hypercritical drying.

Although sample C19 is also cogelled, it exhibits very large Pd particles, the mean size of which is 80.9 nm. Among the four cogelled catalysts examined here, sample C19 is characterized by the lowest ratio $([TEOS]+[SiO_3C_8N_2H_{22}])/[Pd^{2+}]$ which is equal to 31 (Table 6). According to the nucleation hypothesis, this leads to a large number of Pd crystallites and a small SiO_2 particle diameter (7 nm). It then becomes probable that Pd particles are not completely coated with SiO_2. Gaps would exist which allow Pd crystallites to migrate out of SiO_2 particles. The migration and coalescence mechanism can then occur. The huge size of Pd particles in C19 indicates that sintering occurs to a very large extent during hypercritical drying. In their study on the mechanism of aging of supported metal catalysts, Ruckenstein and Dadyburjor (41) point out that migration is size dependent and will be very small for particles larger than about 5 nm. What happens probably in sample C19 is that, as explained by these authors, the larger particles grow because the smaller particles, which migrate much faster, coalesce with them. One has to point out that direct ripening can also take place when a small crystallite comes near to a large one (42).

Since a purpose of this work is to study sintering during hypercritical drying, cogelled catalysts, which were all dried in this way, have been examined just after drying without being calcined (except for the analysis of sample C18 by CO chemisorption, which requires calcination). The situation is different for impregnated catalysts, four of which (I2, I3, I4, and I5) have been dried under vacuum after impregnation. Due to the mild conditions of this drying ($T = 150$°C), Pd particles are probably only formed, at the oxide state, during a calcination step which then becomes necessary. In sample I1, the only one dried in an autoclave after impregnation, Pd crystallite size was measured before and after calcination and no difference was detected. The comparison between impregnated samples I1 and I2 again allows us to show the extent of sintering during hypercritical drying. Mean Pd crystallite sizes have been measured by TEM and image analysis (Table 3). One obtains $d = 24.6$ nm for I1 (which is in agreement with CO chemisorption) and $d = 7.5$ nm for I2. The textures of those two samples are almost identical except in the macroporous domain (Table 5) where it can be seen that hypercritical drying allows us to retain more macropores. The gap between the metal dispersion in samples I1 and I2 is then not due to a difference between textures but can be explained, as for sample C19, by a high mobility of Pd crystallites in the autoclave conditions when those metal particles are not trapped. This leads to the low dispersion observed in sample I1. Although catalysts I2, I3, I4, and I5 have all been dried under vacuum after impregnation, their metal dispersions are very different: $d \approx 7.4$ nm for I2, I3, and $d \approx 4.7$ nm for I4, I5. As has been shown above, samples I2 and I3 on the one hand and samples I4 and I5 on the other hand exhibit very different textures: while the former exhibit a continuous distribution in the mesopore range, the latter do not present any mesopores with a diameter larger than approximately 15 nm (Fig. 9). Although an oxidizing atmosphere would favor Ostwald ripening according to Ruckenstein and co-workers (37), Zou and Gonzalez in their study on the thermal stability of Pd/SiO_2 sol–gel catalysts (46) assume that, at 650°C in an oxidizing atmosphere, sintering occurs by the migration and coalescence mechanism. If we follow this second hypothesis, the smaller size for Pd crystallites in samples I4 and I5 can be explained by the theory of Ruckenstein and Pulvermacher (45) who proposed that when the size of a crystallite is matched to the diameter of the pore, surface diffusion is inhibited and crystal growth does not occur. As can be seen in Fig. 9, this inhibition will appear for the smaller particles in samples I4 and I5 in relation to samples I2 and I3.

The higher monodispersity in Pd particles-size distributions obtained with $SiO_3C_8N_2H_{22}$ (I2 and I4) in relation to NH_3 (I3 and I5) may indicate a more homogeneous distribution of this metal complex on the support surface during impregnation following a better anchoring.

CONCLUSIONS

The use of 3-(2-aminoethyl)aminopropyl-trimethoxysilane ($SiO_3C_8N_2H_{22}$) to form the complex

$Pd^{2+}(SiO_3C_8N_2H_{22})_2$ in an ethanolic solution containing TEOS and aqueous ammonia has allowed us to obtain cogelled catalysts with a very particular structure. It appears indeed that this metal complex acts as a nucleation agent for the formation of the silica particles. The examination of the texture, the metal dispersion, and its localization in cogelled samples leads to the following conclusion: palladium crystallites with a diameter of about 2.2 nm are located inside silica particles exhibiting a monodisperse microporous distribution centered on a hydraulic radius equal to 0.43 nm. The continuous meso- and macropore distribution is located in voids between these particles and between aggregates constituted of these particles. Although Pd particles are located inside SiO_2 particles, their complete accessibility, via the micropore network, has been demonstrated.

Impregnated catalysts have also been synthesized. In the latter, it appears clearly that Pd particles are located outside SiO_2 particles. Samples with various textures have been prepared and it has been shown that the metal dispersion is texture dependent.

The relation between the texture of cogelled and impregnated catalysts and their behavior toward sintering has been studied in detail. If the migration and coalescence of palladium particles is considered as the predominant mechanism responsible for sintering during hypercritical drying as well as during calcination, the following conclusions can be drawn:

(a) Because they are larger than the micropores of the silica particles in which they are located, the palladium crystallites in cogelled samples are trapped and are then unable to migrate. In consequence, those catalysts are sinter-proof during hypercritical drying.

(b) When the Pd particles are not trapped (in impregnated samples or in cogelled ones if Pd is not completely coated with SiO_2), hypercritical drying leads to an extensive sintering. This shows that metal particles are very mobile in the autoclave conditions.

(c) During calcination of impregnated catalysts dried under vacuum, sintering occurs to various extents depending on the support texture. The Pd crystallite size decreases when the pore size distribution is shifted toward the small sizes. This can be explained by the fact that when the size of a crystallite is matched to the diameter of the pore, surface diffusion is inhibited and crystal growth does not occur anymore.

ACKNOWLEDGMENTS

The authors thank the Solvay Company for TEM analysis and CO chemisorption (double adsorption technique), the Fisons Company for CO adsorption isotherm measurements, and Dr. S. Blacher for her precious help with image analysis. B. Heinrichs is grateful to the Fonds pour la Formation à la Recherche dans l' Industrie et dans l' Agriculture, F.R.I.A., for a grant. The Ministère de la Région Wallonne—Direction générale des Technologies et de la Recherche, the Service de la Programmation de la Politique Scientifique, and the Fonds National de la Recherche Scientifique are also greatefully thanked for financial support.

REFERENCES

1. Lopez, T., Asomoza, M., Bosch, P., Garcia-Figueroa, E., and Gomez, R., *J. Catal.* **138**, 463 (1992).
2. Armor, J. N., Carlson, E. J., and Zambri, P. M., *Appl. Catal.* **19**, 339 (1985).
3. Balakrishnan, K., and Gonzalez, R. D., *J. Catal.* **144**, 395 (1993).
4. Lopez, T., Bosch, P., Asomoza, M., and Gomez, R., *J. Catal.* **133**, 247 (1992).
5. Breitscheidel, B., Zieder, J., and Schubert, U., *Chem. Mater.* **3**, 559 (1991).
6. Lopez, T., Romero, A., and Gomez, R., *J. Non-Cryst. Solids* **127**, 105 (1991).
7. Pajonk, G. M., *Appl. Catal.* **72**, 217 (1991).
8. Heinrichs, B., Pirard, J.-P., and Pirard, R., U.S. Patent 5,538,931 (1996).
9. Brinker, C. J., and Scherer, G. W., "Sol–Gel Science: The Physics and Chemistry of Sol–Gel Processing," Academic Press, San Diego, 1990.
10. Griswold, J., Hney, J. D., and Kleyn, V. A., *Ind. Eng. Chem.* **35**, 701 (1943).
11. Brinker, C. J., Keefer, K. D., Schaefer, D. W., and Ashley, C. S., *J. Non-Cryst. Solids* **48**, 47 (1982).
12. Yates, D. J. C., and Sinfelt, J. H., *J. Catal.* **8**, 348 (1967).
13. Lam, Y. L., and Sinfelt, J. H., *J. Catal.* **42**, 319 (1976).
14. Sinfelt, J. H., "Bimetallic Catalysts—Discoveries, Concepts, and Applications," Wiley, New York, 1983.
15. Benson, J. E., Hwang, H. S., and Boudart, M., *J. Catal.* **30**, 146 (1973).
16. Lecloux, A. J., *in* "Catalysis: Science and Technology" (J. R. Anderson and M. Boudart, Eds.), Vol. 2, p. 171. Springer-Verlag, Berlin, 1981.
17. Eischens, R. P., Francis, S. A., and Pliskin, W. A., *J. Phys. Chem.* **60**, 194 (1956).
18. Scholten, J. J. F., and Van Montfoort, A., *J. Catal.* **1**, 85 (1962).
19. Ichikawa, S., Poppa, H., and Boudart, M., *J. Catal.* **91**, 1 (1985).
20. Rieck, J. S., and Bell, A. T., *J. Catal.* **103**, 46 (1987).
21. Joyal, C. L. M., and Butt, J. B., *J. Chem. Soc., Faraday Trans.* **83**, 2757 (1987).
22. Brunauer, S., Deming, L. S., Deming, W. S., and Teller, E., *J. Amer. Chem. Soc.* **62**, 1723 (1940).
23. Rouquerol, J., Avnir, D., Fairbridge, C. W., Everett, D. H., Haynes, J. H., Pernicone, N., Ramsay, J. D. F., Sing, K. S. W., and Unger, K. K., *Pure Appl. Chem.* **66**, 1739 (1994).
24. Lippens, B. C., and de Boer, J. H., *J. Catal.* **4**, 319 (1965).
25. Lecloux, A., and Pirard, J.-P., *J. Colloid Interface Sci.* **70**, 265 (1979).
26. Broekhoff, J. C. P., and de Boer, J. H., *J. Catal.* **9**, 8 (1967).
27. Broekhoff, J. C. P., and de Boer, J. H., *J. Catal.* **9**, 15 (1967).
28. Broekhoff, J. C. P., and de Boer, J. H., *J. Catal.* **10**, 153 (1968).
29. Fricke, J., *in* "Aerogels: 1st International Symposium Proceedings, Würzburg, Sept. 23–25, 1985" (J. Fricke, Ed.), Proceedings in Physics, Vol. 6, p. 2. Springer-Verlag, Berlin, 1986.
30. Mikhail, R. S., Brunauer, S., and Bodor, E. E., *J. Colloid Interface Sci.* **26**, 45, 54 (1968).
31. Brunauer, S., *Chem. Eng. Prog. Symp. Ser. 96* **65**, 1 (1969).
32. Washburn, E. W., *Proc. Natl. Acad. Sci.* **7**, 115 (1921).
33. Pirard, R., Blacher, S., Brouers, F., and Pirard, J.-P., *J. Mater. Res.* **10**, 2114 (1995).
34. Pirard, R., Heinrichs, B., and Pirard, J.-P., Communication at the "4th International Symposium on the Characterization of Porous Solids, COPS-IV, Bath, Sept. 15–18, 1996" [also *in* "Characterization of

Porous Solids IV," The Royal Society of Chemistry, London, to appear].
35. Schmidt, H., and Scholze, H., *in* "Aerogels: 1st International Symposium Proceedings, Würzburg, Sept. 23–25, 1985" (J. Fricke, Ed.), Proceedings in Physics, Vol. 6, p. 49. Springer-Verlag, Berlin, 1986.
36. Schubert, U., Breitscheidel, B., Buhler, H., Egger, C., and Urbaniak, W., *in* "Symposium Proceedings, Better Ceramics Through Chemistry V, San Francisco, April 27–May 1, 1992" (M. J. Hampden-Smith, W. G. Klemperer, and C. J. Brinker, Eds.), Materials Research Society Symposium Proceedings, Vol. 271, p. 621. Materials Research Society, Pittsburgh, 1992.
37. Stevenson, S. A., Dumesic, J. A., Baker, R. T. K., and Ruckenstein, E., "Metal-Support Interactions in Catalysis, Sintering, and Redispersion," Van Nostrand–Reinhold, New York, 1987.
38. Ruckenstein, E., and Pulvermacher, B., *J. Catal.* **29**, 224 (1973).
39. Ruckenstein, E., and Pulvermacher, B., *AIChE J.* **19**, 356 (1973).
40. Pulvermacher, B., and Ruckenstein, E., *J. Catal.* **35**, 115 (1974).
41. Ruckenstein, E., and Dadyburjor, D. B., *J. Catal.* **48**, 73 (1977).
42. Ruckenstein, E., and Dadyburjor, D. B., *Thin Solid Films* **55**, 89 (1978).
43. Chen, J. J., and Ruckenstein, E., *J. Catal.* **69**, 254 (1981).
44. Ruckenstein, E., and Dadyburjor, D. B., *Rev. Chem. Eng.* **1**, 251 (1983).
45. Ruckenstein, E., and Pulvermacher, B., *J. Catal.* **37**, 416 (1975).
46. Zou, W., and Gonzalez, R. D., *Appl. Catal. A* **126**, 351 (1995).